A 300-year tree-ring δ^{18}O-based precipitation reconstruction for the South American Altiplano highlights decadal hydroclimate teleconnections

Check for updates

Milagros Rodriguez-Caton [1,2,3] ✉, Mariano S. Morales[2,4], Mukund Palat Rao [1,3,5], Troy Nixon[1,5], Mathias Vuille [6], Juan Antonio Rivera [2], Rose Oelkers[1], Duncan A. Christie [7,8,9], Arianna M. Varuolo-Clarke [1], M. Eugenia Ferrero[2,4], Troy Magney[3], Valérie Daux [10], Ricardo Villalba[2,9] & Laia Andreu-Hayles [1,5,11]

Tropical South American climate is influenced by the South American Summer Monsoon and the El Niño Southern Oscillation. However, assessing natural hydroclimate variability in the region is hindered by the scarcity of long-term instrumental records. Here we present a tree-ring δ^{18}O-based precipitation reconstruction for the South American Altiplano for 1700–2013 C.E., derived from *Polylepis tarapacana* tree rings. This record explains 56% of December–March instrumental precipitation variability in the Altiplano. The tree-ring δ^{18}O chronology shows interannual (2–5 years) and decadal (~11 years) oscillations that are remarkably consistent with periodicities observed in Altiplano precipitation, central tropical Pacific sea surface temperatures, southern-tropical Andean ice core δ^{18}O and tropical Pacific coral δ^{18}O archives. These results demonstrate the value of annual-resolution tree-ring δ^{18}O records to capture hydroclimate teleconnections and generate robust tropical climate reconstructions. This work contributes to a better understanding of global oxygen-isotope patterns, as well as atmospheric and oceanic processes across the tropics.

The hydroclimate of tropical South America is modulated by the South American Summer Monsoon (SASM) which in turn can be largely influenced by the El Niño Southern Oscillation (ENSO)[1,2]. Extreme precipitation and drought events, resulting from the combined influence of ENSO and SASM variability, affect human activities and ecosystems in tropical and subtropical South America. Major droughts have severe environmental and socioeconomic consequences with agricultural losses threatening food security[3,4]. The effects of floods, caused by extreme precipitation events, include population displacement, poor sanitation, land degradation and infrastructure damage, among others[5,6]. In the

southern tropical Andes (~8°S–24°S), climate is particularly variable in time and space due to the interaction between the atmospheric circulation and the complex topography of the region. Additionally, due to a paucity of multi-decadal instrumental observations, characterisation of natural variability is highly uncertain, complicating the assessment of current and future changes in hydroclimatic conditions[7-10]. Paleoclimatic records located in the southern tropical Andes are key to reconstruct local and regional hydroclimate, determine the driving mechanisms of recent variability, and provide information to validate global climate models.

[1]Lamont-Doherty Earth Observatory of Columbia University, Palisades, NY 10964, USA. [2]Instituto Argentino de Nivología, Glaciología y Cs. Ambientales (IANIGLA), CONICET, Mendoza, Argentina. [3]Department of Plant Sciences, University of California, Davis, CA 95616, USA. [4]Laboratorio de Dendrocronología, Universidad Continental, Huancayo, Peru. [5]CREAF, Bellaterra, Barcelona, Spain. [6]Department of Atmospheric and Environmental Sciences, State University of New York at Albany, Albany, NY, USA. [7]Laboratorio de Dendrocronología y Cambio Global, Instituto de Conservación Biodiversidad y Territorio, Universidad Austral de Chile, Valdivia, Chile. [8]Center for Climate and Resilience Research, (CR)2, Santiago, Chile. [9]Cape Horn International Center (CHIC), Punta Arenas, Chile. [10]Laboratoire des Sciences du Climat et de l'Environnement, CEA/CNRS/UVSQ/IPSL, Gif-sur-Yvette, France. [11]ICREA, Pg. Lluís Companys 23, Barcelona, Spain. ✉e-mail: milagrosrodriguezc@gmail.com

Stable oxygen isotope records (δ^{18}O) retrieved from natural archives such as tree rings, corals, ice cores, speleothems, and lake sediments, contain valuable information on local and regional hydroclimate variations[11]. Coral δ^{18}O records in the tropical Pacific Ocean have provided insights on ENSO variability[12–14] as well as decadal teleconnections between Atlantic and Pacific Oceans in the last century[15]. Ice core, speleothem, and lake sediment δ^{18}O records in the tropical Andes have been successfully utilised to report past hydroclimate variability at centennial to multi-millennial time scales[16–18]. Tree-ring δ^{18}O records have demonstrated potential to assess annual-resolution hydroclimate changes for the last 40–200 years in tropical South America[19–26]. However, multi-century climate reconstructions based on tree-ring δ^{18}O chronologies have not yet been developed for the Altiplano, a high-elevation plateau located in the southern tropical Andes.

In the South American Altiplano, more than 80% of the annual precipitation falls during December, January, February, and March (DJFM), coincident with the mature phase of the SASM[27]. Most moisture that feeds this summer precipitation is sourced from air masses originating in the tropical Atlantic Ocean, recycled over the Amazon basin and transported toward the Altiplano[10,28]. Prevailing easterly winds at lower to middle levels of the troposphere (~925–500 hPa) transport moisture towards the continental interior and upslope of the Andes[29]. Precipitation events during summer are related to the formation of the Bolivian High, an upper-level (~200 hPa) anticyclonic circulation over Bolivia, that facilitates the moisture transport to the eastern flanks of the Andes along its northern side.

Conversely, dry periods during the summer are tied to anomalous intensification of upper-level westerly winds[30]. At interannual timescales, sea surface temperature (SST) anomalies in the Pacific and Atlantic Oceans perturb the atmospheric circulation and influence precipitation over the Altiplano. Warmer than average central Pacific SST (i.e. El Niño-related anomalies) tends to favour upper-tropospheric westerlies aloft the Altiplano and the anomalous Walker circulation promotes subsidence over the western equatorial Atlantic and the SASM regions, thereby reducing moisture influx from the Atlantic toward the Amazon basin and the Altiplano[2,31].

The tree-ring δ^{18}O record retrieved from *Polylepis tarapacana*, a species distributed across the South American Altiplano, has recently emerged as a proxy for precipitation variability over the Altiplano[32,33]. This record reflects a combination of isotopic fractionation (Rayleigh distillation) over the south-western Amazon basin upstream of the Altiplano, local precipitation amount, and other processes before and after plant water uptake that enhance the precipitation signal[33]. Through Rayleigh distillation the $H_2^{18}O$ isotopologues of water, with lower saturation vapour pressure and heavier mass than $H_2^{16}O$, condensate and precipitate preferentially. Strong convection and precipitation over the Amazon during the SASM largely aid in the removal of heavy water isotopologues from the air mass, and the remaining water vapour has a lower $^{18}O/^{16}O$ ratio than the water that condenses as rain. As precipitation increases upstream of the Altiplano (i.e. Bolivian lowlands and southwestern Brazil), the remaining water vapour becomes more depleted in heavy isotopes (e.g. refs. [34–36]). Thus, in years
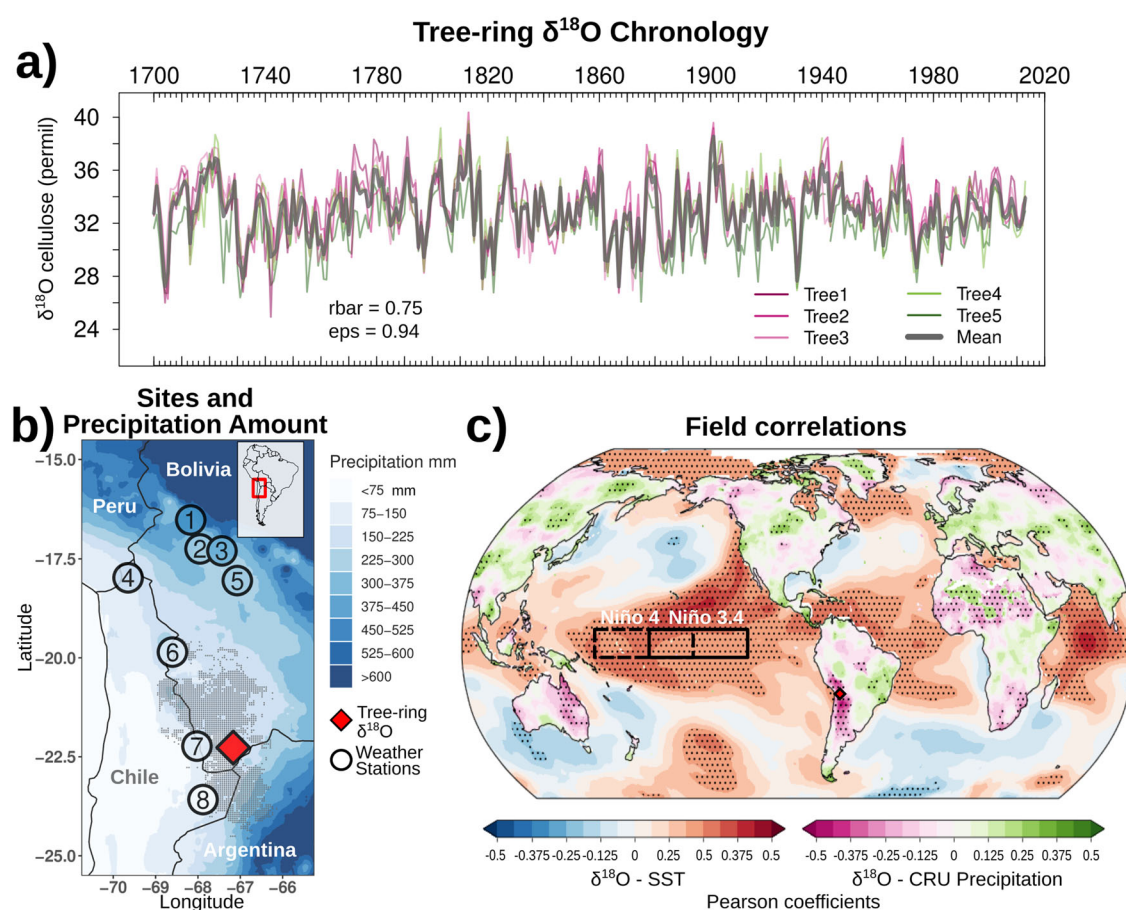
Fig. 1 | Tree-ring δ^{18}O chronology and field correlations with sea surface temperature (SST) anomalies and precipitation anomalies. a Tree-ring δ^{18}O series from five individual trees (thin lines), and the average tree-ring δ^{18}O chronology (thick line) for the period 1700–2013. **b** Location of the *Polylepis tarapacana* tree-ring δ^{18}O site (red diamond) and weather stations (black circles) used in the precipitation reconstruction (see Table 1 for more details). Background colours in **b** represent mean summer (DJFM) precipitation from CHIRPS (shading) and weather stations (circles, as shaded in-fill), for the common period 1982–1993. Dotted area in **b** corresponds to the DJFM CHIRPS precipitation grid cells that are highly correlated ($p < 0.001$) with our δ^{18}O series and were used to re-scale the precipitation departures to millimetres (see methods). **c** Field correlations between the *Polylepis tarapacana* δ^{18}O chronology and DJFM SST and DJFM CRU precipitation over land for the period 1901 to 2013. Dotted areas in **c** indicate significant correlations ($p < 0.05$).

with enhanced rainout upstream, the depleted water vapour in the air masses that further reach the Altiplano will condensate as precipitation, leading to a more negative isotopic composition of precipitation (δ^{18}Op) in this region[33]. This δ^{18}Op signal is further combined with a local precipitation-amount effect, whereas more precipitation over the Altiplano results in more depleted δ^{18}Op[33]. Indeed, annual δ^{18}Op minima are coincident with annual maxima in easterly winds, increased deep convection and local annual precipitation maxima[37].

The absolute δ^{18}O values in plants differ from δ^{18}Op due to evaporative fractionation processes before and after plant water uptake[38]. The infiltrated surficial water carrying the δ^{18}Op signal can become enriched in ^{18}O as a result of evaporation (i.e. $H_2^{16}O$ evaporates preferentially due to its lighter weight[39]). Soil water is then absorbed by the roots and transported through the xylem towards the leaves. Because no fractionation takes place during plant water uptake, xylem and soil water share the same δ^{18}Op signal. Evaporative fractionation at the leaf level occurs during transpiration through the stomata. This evapotranspiration process can therefore increase the proportion of the heavy isotope in the leaf water and subsequent sugars formed during photosynthesis[40]. Finally, during cellulose formation, oxygen exchanges between intermediate sugar components and xylem water can occur (e.g. ref. 41), a process that can reinforce the δ^{18}Op signal in tree-ring cellulose because, as stated above, xylem and soil water have similar δ^{18}Op signals.

In the South American Altiplano, the existence of the long-lived tree species *Polylepis tarapacana*, which can reach an age up to 750 years[42], has enabled the development of multi-century hydroclimate reconstructions based on its ring-width variability[43,44]. While tree-ring width of this species is related to previous growing season precipitation[45], the tree-ring δ^{18}O of *Polylepis tarapacana* is sensitive to current growing-season climate, showing strong negative correlations with rainfall during the current growing season[32,33]. This relationship between growing season precipitation and tree-ring δ^{18}O was shown to be consistent along a latitudinal-aridity gradient across the Altiplano[32], with the highest correlations occurring within the summer rainy season in January, February and March (JFM), providing initial evidence that tree-ring δ^{18}O may be a powerful proxy to understand both past and present precipitation variability across the Altiplano. The climate signal recorded in the *Polylepis tarapacana* tree-ring δ^{18}O provides a new opportunity to develop complementary precipitation reconstructions for this tropical Andean region. Here we use tree-ring δ^{18}O to reconstruct SASM season precipitation in the southern tropical Andes from 1700 to 2013. Our tree-ring δ^{18}O-based reconstruction captures easterly 200 hPa wind flow and convective activity related with precipitation events over the Altiplano region. Interannual (2–5 years) and decadal (~11 years) oscillations in the record are shared with instrumental precipitation and tropical Pacific SST in the Niño 3.4 and Niño 4 regions. The tree-ring δ^{18}O decadal frequency is remarkably consistent with decadal periodicities in southern-tropical Andean ice core δ^{18}O and tropical Pacific coral δ^{18}O archives, demonstrating the capacity of δ^{18}O records to capture decadal-scale hydroclimate teleconnections. The high sensitivity to SASM and SST interannual and decadal variability highlights the value of tree-ring δ^{18}O records to generate more robust tropical climate reconstructions.

Results

Signal-strength of the tree-ring δ^{18}O chronology

Analysing individual and annually resolved tree-ring series is essential in dendrochronological research because it allows to assess the strength of the common signal shared by individual series and the quality of the record through time. The tree-ring δ^{18}O chronology, based on individual tree-ring δ^{18}O series from five *Polylepis tarapacana* trees, shows an average correlation coefficient between trees (rbar) of 0.75 and expressed population signal (EPS) of 0.94 for the entire period 1700–2013 (Fig. 1a). These statistics indicate a common signal shared between individual δ^{18}O tree series, likely reflecting a strong climate signal retained by the δ^{18}O chronology through time. This common climate signal is reflected by significant correlations between the tree-ring δ^{18}O chronology and gridded precipitation datasets

Table 1 | Precipitation records from meteorological stations selected for the reconstruction, and their correlations with the *Polylepis tarapacana* δ^{18}O chronology for the common period

Meteorological Station	Country (Source)	Elevation m a.s.l.	Latitude °S	Longitude °W	Distance to Study site km	Mean Precip 1982–1993 mm	Common period with δ^{18}O	Number of years	Pearson r with δ^{18}O Comm. period	T value with δ^{18}O Comm. period	Average Pearson r with other stations 1982–1993	Pearson r with regional mean 1982–1993
1- La Paz	Bolivia(a)	4060	16.52	68.17	640	402	1949–2001	53	−0.55***	56	0.64	0.81***
2- Patacamaya	Bolivia(a)	3789	17.25	67.95	563	255	1946–1993	48	−0.35**	40	0.57	0.78***
3- Puchuni	Bolivia(c)	4208	17.3	67.43	548	310	1982–2002	21	−0.59***	47	0.64	0.92***
4- Alcerreca	Chile(b)	3900	17.98	69.65	535	217	1972–2008	37	−0.31*	61	0.50	0.66**
5- Oruro	Bolivia(a)	3702	18.05	67.07	458	295	1944–1998	55	−0.58***	66	0.69	0.92***
6- Cancosa	Chile(b)	3930	19.85	68.60	301	149	1977–2011	35	−0.56***	112	0.73	0.93***
7- Linzor	Chile(b)	4100	22.23	68.02	86	135	1975–2014	35	−0.63***	100	0.66	0.91***
8- Socaire	Chile(b)	3251	23.58	67.88	159	30	1975–2014	39	−0.62***	136	0.67	0.89***

Stations are ordered and numbered from north to south according to Fig. 1b. The source of information is depicted between brackets next to the country of location of each station. Mean precipitation was calculated between 1982 and 1993, the period of overlap among all meteorological records. The common period between each station and the δ^{18}O chronology is indicated, followed by the length of the stations, the Pearson correlation coefficient with δ^{18}O, and T values, over this common period. The average Pearson correlation coefficient between each station and their neighbours, and the Pearson correlation coefficient between each station and the regional-mean precipitation series used for the reconstruction, are also indicated for 1982–1993.
Comm. Period common period.
*p < 0.1; **p < 0.05; ***p < 0.001.
(a)SENAMHI: Servicio Nacional de Meteorología e Hidrología, Bolivia.
(b)DGA: Dirección General de Aguas, Chile.
(c)Ref. 101.

across the southern tropical Andes (Fig. 1b, c) and gridded SST in the central tropical Pacific (Fig. 1c) during the summer season. The tree-ring $\delta^{18}O$ chronology is negatively correlated with DJFM precipitation from the Climate Research Unit (CRU) and the Climate Hazards Group InfraRed Precipitation with Station (CHIRPS) (Fig. 1b, c). Figure 1c shows that tree-ring $\delta^{18}O$ provides a good spatial representation of CRU rainfall across the Altiplano for the period 1901–2013, with significant correlations covering areas of southern Peru, northern Chile, western Bolivia and northwestern Argentina, also expanding into central Argentina. The tree-ring $\delta^{18}O$ chronology is positively related with DJFM SST across tropical regions, most significant in the central Pacific, western tropical Atlantic and western Indian Ocean, for the period 1901–2013 (Fig. 1c). These results reveal local, regional and global scale hydroclimate variability imprinted in the $\delta^{18}O$ chronology.

Interannual and decadal climate signal of the tree-ring $\delta^{18}O$ chronology

Using multi-taper and wavelet methods we identify interannual to decadal periodicities in the tree-ring $\delta^{18}O$ and instrumental data. The multi-taper method identifies significant interannual (2–5 years) oscillations in our tree-ring $\delta^{18}O$ chronology over the period 1700–2013 (Fig. 2a). Consistent with these results, the wavelet analysis of our tree-ring $\delta^{18}O$ chronology shows similar results at the interannual time scale (Fig. 2b). A similar interannual oscillatory peak (3 years) is shown in Fig. 2c for the observed 1961–2007

precipitation record (>90% confidence level). As expected, SSTs in the Niño 3.4 and Niño 4 regions have significant (>95% confidence level) interannual oscillatory peaks of 2–7 years for 1854–2019 (Fig. 2c). We find a prominent 10–11-year spectral peak in our tree-ring $\delta^{18}O$ chronology (Fig. 2a, b). Decadal-interdecadal frequencies from 10 to 14 years are also significant for SST in the Niño 3.4 region (>90% confidence level), and particularly prominent for SST in the Niño 4 region (>95% confidence level) (Fig. 2c).

The consistency between the instrumental records and the tree-ring $\delta^{18}O$ chronology is further supported by the results of the wavelet coherence analysis (Fig. 2d, e). The tree-ring $\delta^{18}O$ chronology is significantly antiphased with DJFM instrumental precipitation at interannual (2–7 years) and decadal (8–16 years) time scales (Fig. 2e). At interannual periods (2–6 years) tree-ring $\delta^{18}O$ is in-phase with SSTs in the Niño 3.4 and Niño 4 regions, while at decadal (8–16 years) and multidecadal (16–32 years) periods it is more related with SST in the Niño 4 region (Fig. 2d, e). These results collectively indicate that the interannual and decadal properties of the instrumental precipitation and SST records are well reflected in our tree-ring $\delta^{18}O$ record.

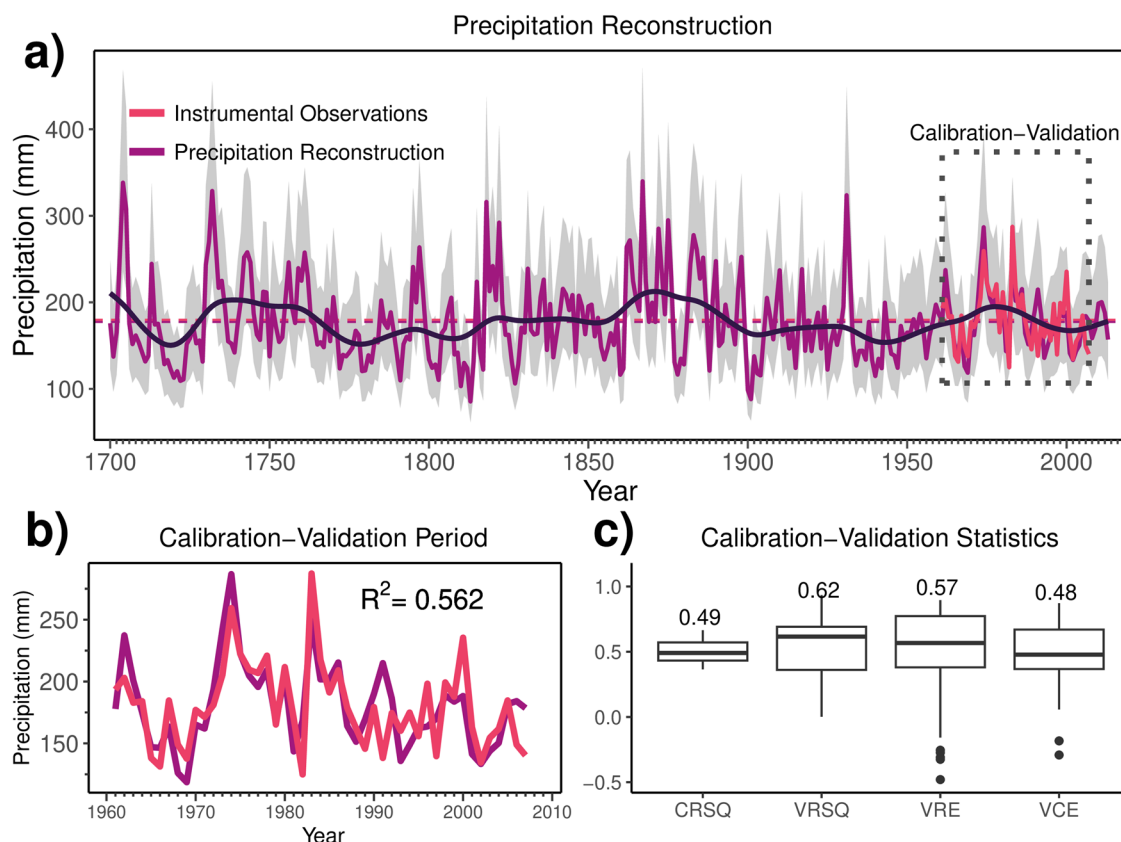### The precipitation reconstruction
A skilful summer precipitation reconstruction for the period 1700–2013 was developed from the tree-ring $\delta^{18}O$ chronology derived from five *Polylepis tarapacana* tree individuals (Fig. 3). The final R^2 between our tree-ring $\delta^{18}O$
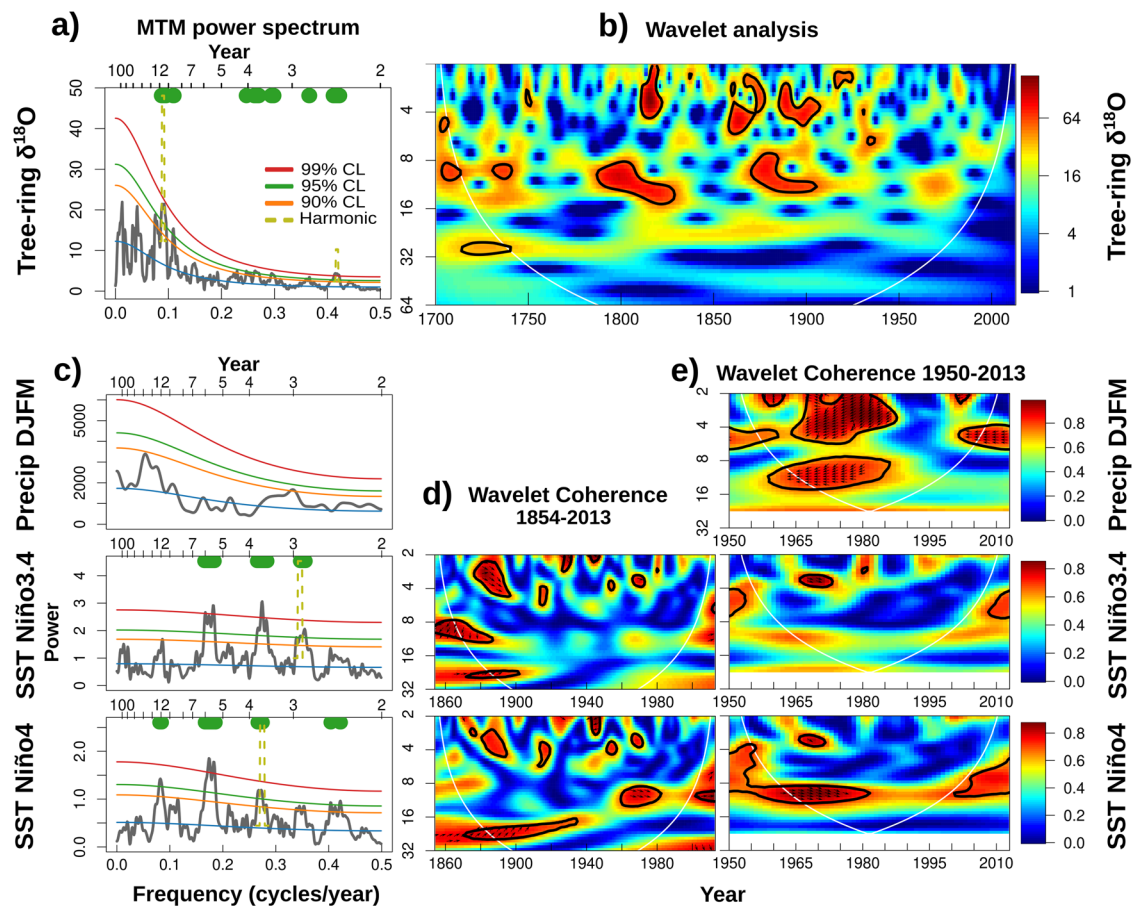
Fig. 2 | Spectral properties of the tree-ring $\delta^{18}O$ chronology and instrumental records. a Multi-taper-method (MTM) power spectrum for $\delta^{18}O$ chronology for the period 1700–2013. **b** Wavelet analysis for the $\delta^{18}O$ chronology. **c** MTM power spectrum for instrumental precipitation for 1950–2008, and SST in the Niño 3.4 and Niño 4 regions for 1854–2019. In **a** and **c** continuous lines represent confidence levels determining significant spectral peaks, with colours indicating 90 (orange), 95 (green) and 99% (red) confidence levels. Dashed lines in **a** and **c** represent harmonic peaks in the time series for a given cycle. In **a** and **c** filled green circles highlight

spectral peaks exceeding the 95% confidence level. **d** Wavelet coherence and phase spectrum for the period 1854–2013 between our $\delta^{18}O$ chronology and SST in the Niño 3.4 and Niño 4 regions. **e** Wavelet coherence and phase spectrum for the period 1950–2013 between our $\delta^{18}O$ chronology and instrumental precipitation, and SST in the Niño 3.4 and Niño 4 regions. In **d** and **e** black arrows pointing right and left indicate phased (i.e. positively correlated) and antiphased (i.e. negatively correlated) relationships, respectively.

Fig. 3 | Altiplano precipitation reconstruction and related statistics. a DJFM precipitation reconstruction for the period 1700–2013 based on *Polylepis tarapacana* tree-ring δ^{18}O. The purple and pink dashed lines represent the median of the reconstruction and instrumental series, respectively, and the grey shading depicts the 95% confidence interval for the 38 leave-10-out models. **b** Observed and reconstructed precipitation for the calibration-validation period 1961–2007 and the r-squared between the two time series. **c** Summary of reconstruction calibration-validation statistics for the 38 models: calibration r-squared (CRSQ); validation r-squared (VRSQ); validation reduction of error (VRE) and verification coefficient of efficiency (VCE). Each box describes the median (thick line), and the 25th and 75th percentiles of the data; and whiskers correspond to ±1.5 of the inter-quantile range.

Table 2 | Individual years and periods with extreme hydroclimatic conditions according to the δ^{18}O-based DJFM precipitation reconstruction

Extreme years				Consecutive periods		Periods >9 years	
DRY		**WET**		**DRY**	**WET**	**DRY**	**WET**
Percentile 5		Percentile 95		Percentile 10	Percentile 90	Lower than mean	Higher than mean
1720	**1860**	1704	1862	1719–1723	1703–1705	**1709–1727**	**1700–1708**
1722	1878	1705	1863	**1779–1780**	1730–1733	**1766–1818**	1728–1765
1723	1900	1731	1867	1810–1813	1742–1744	1895–1964	1819–1849
1791	1901	1732	1872	**1860–1861**	1862–1863	1992–2012	1855–1894
1803	1903	1733	1875	1900–1901	1882–1884		1965–1991
1810	1904	**1797**	1883	1902–1904	1973–1974		
1813	1940	1818	1931				
1827	1969	1822	1974				

Extreme years represent extreme dry (5th percentile) or wet (95th percentile) years. Consecutive periods represent continuous periods of two to five years with dry (10th percentile) or wet (90th percentile) conditions. Periods >9 years represent periods of nine or more years with overall below- or above-average precipitation conditions. Bold values represent droughts and floods reported in historical information (see Discussion section).

precipitation reconstruction and the instrumental precipitation period 1961–2007 is 0.56, indicating that the reconstruction explains 56% of the precipitation variability in this region (Fig. 3 a, b). The robustness of the precipitation reconstruction can be further evaluated by calculating the coefficients of determination (r-squared) during multiple block calibration and verification periods (see Methods). The median calibration r-squared (CRSQ) for the 38 participating models is 0.49 during the 37-year

calibration period, and the median verification r-squared (VRSQ) for the 38 participating models is 0.62 over the 10-year verification period (Fig. 3c). Positive median values of the reduction of error statistic (VRE = 0.55), and the coefficient of efficiency (VCE = 0.43) further support the robustness of this reconstruction.

Table 2 shows the extreme years and periods with below and above average precipitation from our reconstruction. Consecutive years of low
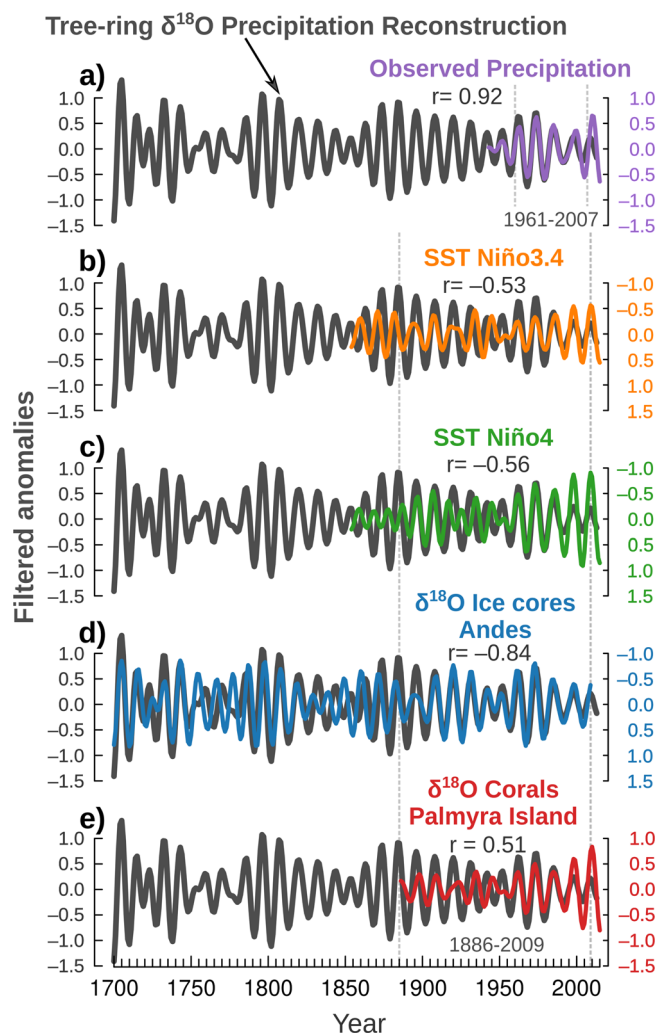
Fig. 4 | Decadal anomalies for instrumental- and paleo-records. Decadal anomalies of the tree-ring δ^{18}O-based precipitation reconstruction (black line), compared with decadal anomalies of **a** Instrumental observations of precipitation based on the target meteorological stations utilised for the calibration (1943–2013); **b** SST anomalies for the Niño 3.4 and **c** Niño 4 regions for the period 1854–2019[85]; **d** Andean ice core δ^{18}O record covering the period 1700–2009, obtained by combining ice core δ^{18}O records from Quelccaya (400–2009 CE)[17], Huascaran (1894–1992 CE)[94], and Sajama (1949–1997 CE)[95]; **e** Coral δ^{18}O record from Palmyra Island in the tropical Pacific covering the period 1886–2016[15,96]. Decadal anomalies were calculated using a 9–14-year band-pass filter. Note that the Y-axes for the filtered SST and ice core δ^{18}O have been inverted to facilitate visual comparison. All Pearson correlation coefficients (r) are significant ($p < 0.001$). Vertical lines indicate the period used for the calculation of r.

precipitation values (<0.1 percentile) include 1719–1723, 1779–1780, 1810–1813, 1860–1861, 1900–1901, 1902–1904. Consecutive years of high precipitation values (>0.9 percentile) include 1703–1705, 1730–1733, 1742–1744, 1862–1863, 1882–1884, 1973–1974. Long periods of overall dry conditions (lower than the mean and lasting more than 9 years) include 1709–1727, 1766–1818, 1895–1964, 1992–2012. Long periods of overall wet conditions (higher than the mean) lasting 9 or more years, include 1700–1708, 1728–1765, 1819–1849, 1855–1894, 1965–1991.

The precipitation reconstruction and its relation with instrumental observations and paleo-proxies

Based on the decadal signal shared by the tree-ring δ^{18}O and instrumental data (Fig. 2), a band-pass filter of 9–14 years was applied to tree-ring δ^{18}O-based

reconstructed and instrumental precipitation, SST in El Niño regions, ice core and coral δ^{18}O paleo-records. The 9–14 year filtered precipitation reconstruction is consistent with the filtered series of instrumental precipitation (r = 0.92 for the calibration-validation period 1961–2007), Pacific SST over the Niño 3.4 (r = −0.53) and Niño 4 (r = −0.56) regions, as well as the Central-Andean ice core δ^{18}O (r = 0.84) and the tropical Pacific coral δ^{18}O records (r = 0.51) (Fig. 4). For the correlation coefficients to be comparable, the Pearson correlation coefficient is calculated for the common period 1886–2009, except for the instrumental precipitation which is calculated over the period 1961–2007. All Pearson correlation coefficients (r) are significant at the 99% significance level, considering the effective numbers of degrees of freedom (Eq. (1)).

The 9–14-year filtered DJFM precipitation reconstruction adequately represents the amplitude of instrumental precipitation variations (Fig. 4a). The amplitude of tropical Pacific SST is also well represented, particularly during the last century, although a decoupling between the phasing of the time series is evident during 1930–1950 (Fig. 4b, c), also present in the δ^{18}O Pacific coral records (Fig. 4e). The amplitude of the decadal variability of the precipitation reconstruction is coherent with the δ^{18}O Central-Andean ice core record during 1700–1750, around 1800s and after the 1900s (Fig. 4d).

Gridded datasets for precipitation, Outgoing Longwave Radiation (OLR), and 200 hPa zonal and meridional winds, were correlated and regressed separately with instrumental DJFM precipitation (Fig. 5a–c) and our reconstruction (Fig. 5d–f) for the period 1981–2013. The results reveal that our reconstruction has similar regional correlation patterns as the instrumental data. As expected, the instrumental record is consistent with gridded precipitation over the Altiplano, as shown by the significant and positive correlations with the CHIRPS dataset (Fig. 5a). This relationship, found using the instrumental record, is also shared by our precipitation reconstruction and it extends towards the Amazon region in both cases, although our reconstruction reported weaker correlations in this region (Fig. 5d).

Negative correlations between our instrumental DJFM precipitation record and the OLR field are indicative of enhanced convective activity associated with periods of stronger rainfall, at local to regional spatial scales (Fig. 5c). In line with the results for gridded precipitation, the signal over the Amazon basin is present in the instrumental correlation (Fig. 5c) but weaker in our reconstruction (Fig. 5f). One of the main drivers for local convection is the anomalous easterly flow over the latitudinal band aloft the Altiplano, a signal that is observed in both instrumental and reconstructed records considering the regression field with the upper-level winds at 200 hPa (Fig. 5b, e).

Field correlations between our tree-ring δ^{18}O-based DJFM precipitation reconstruction and the reconstructed Palmer Drought Severity Index (PDSI) for the period 1700–1999 show a remarkable regional consistency (Fig. 6) between these two records. Positive correlation coefficients of r ~ 0.4 are shown for the period 1700–1999 for the Altiplano of Peru, Bolivia, Chile, and Argentina, but also over adjacent lowland areas of Bolivia, northwestern Argentina and northwestern Paraguay. Significant negative correlation coefficients are found over south-eastern Paraguay, south-eastern Brazil, northern Uruguay and the northeastern tip of Argentina, capturing the summer west-east rainfall dipole pattern in tropical South America.

Discussion

Assessing natural precipitation variability and the role of tropical Pacific Sea Surface Temperatures (SST) on tropical South American hydroclimate is hindered by the scarcity of long-term instrumental records. Here we present an annually resolved tree-ring δ^{18}O-based precipitation reconstruction for the South American Altiplano for the period 1700–2013 C.E. The precipitation record is developed by measuring the δ^{18}O in cellulose from individual tree rings of five *Polylepis tarapacana* trees, and subsequently analysing the climate signal embedded in the resulting chronology. The reconstruction explains 56% of variability of the summer (DJFM) precipitation instrumental record and faithfully represents its relationships with general atmospheric circulation patterns. Our tree-ring δ^{18}O precipitation reconstruction shows a good agreement with observed local-to-
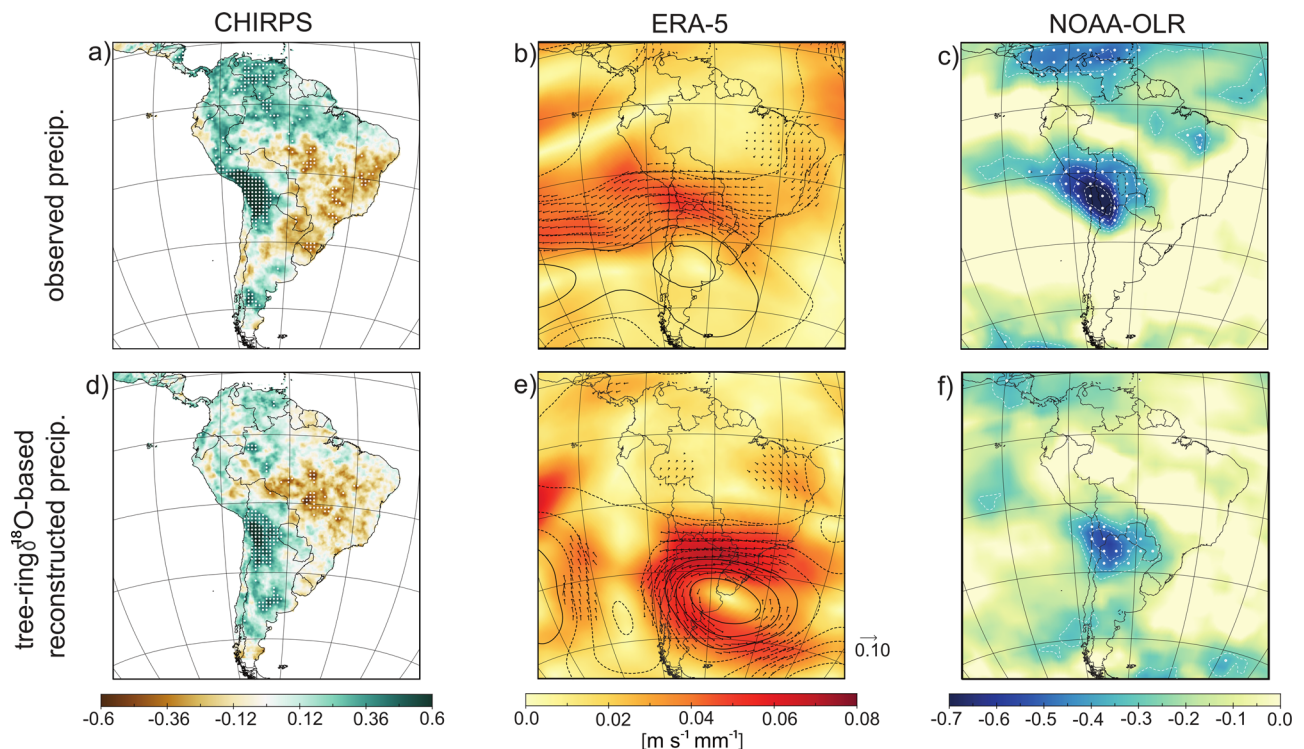
Fig. 5 | Regional atmospheric patterns and comparisons between observed and tree-ring δ^{18}O- based reconstructed summer precipitation. a DJFM instrumental precipitation correlated against DJFM CHIRPS precipitation. Regions with significant correlations ($p < 0.05$) are indicated with white stippling. **b** As in **a** but regressed against 200 hPa wind field and geopotential height (ERA5). Colour shading indicates wind speed regression coefficient [m s^{-1} mm^{-1}]. Wind vectors are only plotted where either zonal or meridional component is significantly correlated with instrumental precipitation. Contour interval for geopotential height is 0.1 m mm^{-1} and negative contours are dashed. **c** As in **a** but correlated against interpolated OLR. Regions with significant correlations ($p < 0.05$) are indicated with white stippling. Dashed contours indicate r-values < -0.3, with contour interval of 0.1. Only negative correlations are plotted. **d–f** As in **a–c** but for δ^{18}O-reconstructed precipitation. Time period for all analyses is 1981–2013.

regional precipitation and tropical Pacific SST, as well as independent tree-ring width, ice core δ^{18}O and coral δ^{18}O paleorecords, highlighting its value as a paleoproxy for Altiplano precipitation and its regional forcings.

Three hundred years of Altiplano hydroclimate variability inferred from δ^{18}O in tree rings

Atmospheric and hydroclimatic processes, such as precipitation amount, condensation temperature, and distance to the moisture source, affect the isotopic composition of precipitation (e.g. ref. [46]). These environmental signals contained in δ^{18}Op can further be imprinted in natural archives. For example, plants can retain the δ^{18}Op signal because plant roots absorb soil water that originates from precipitation. This water is used for different plant processes, including synthesis of sugars (e.g. cellulose) that are further used for wood formation (i.e. tree rings). Thus, δ^{18}O values measured in tree-ring cellulose can reflect environmental processes at local (e.g., local precipitation amount, evaporation and plant transpiration) and regional scales (e.g. upstream rainout).

Annual to seasonal information of past hydroclimate variability has been provided by tree-ring δ^{18}O records in different regions of South America[19–22,24,25,47–53]. It has been previously demonstrated that *Polylepis tarapacana* tree-ring δ^{18}O chronologies located in the southern Altiplano register local and regional hydroclimate variability. The longevity of *Polylepis tarapacana* and the sensitivity of its tree-ring δ^{18}O chronologies to local and regional hydroclimate variability[19,33], allowed us to develop an annually resolved 300-year record of precipitation variability, to our knowledge the longest tropical tree-ring δ^{18}O chronology in the Southern Hemisphere north of 23°S.

Consistent with previous findings over the instrumental period[19,32,33], tree-ring δ^{18}O is negatively correlated with regional summer (DJFM)

precipitation (Fig. 1c). This is also in agreement with other δ^{18}O records in this region and can be interpreted as the result of Rayleigh distillation and upstream rainout of the water sourced from the Atlantic, recycled over the Amazon and transported to the southeast via the low-level jet along the eastern flank of the Andes[18,36,54,55].

The PDSI field reconstruction from the SADA and our tree-ring δ^{18}O-based precipitation reconstruction show a remarkably high spatial consistency across the entire Altiplano, and lowland areas of Bolivia and northwestern Argentina (Fig. 6). The SADA is a gridded record of past drought conditions expressed by the PDSI based on a network of South American tree-ring width chronologies located poleward of 12°S. The SADA is an appropriate product to compare with our δ^{18}O-based reconstruction due to its complete spatiotemporal coverage across southern South America[56]. The SADA ring-width records originate from several species, including species growing in the Altiplano as well as other species from the Bolivian and northwestern Argentinean lowlands. While the *Polylepis tarapacana* ring-width record from the Uturunco site is included in the SADA, we note that the Uturunco's tree-ring δ^{18}O is different and independent from the ring-width record[32] and is not included in the SADA.

According to historical archives that extend back to the 14th century[57,58], large regional droughts occurred over the region during 1779–1780, 1791, and 1802–1804, named the Silver Mine drought[57–59]. Our precipitation reconstruction recorded these extreme events and overall dry conditions represented by the lowest precipitation percentiles (e.g. 1779–1780, 1791, 1803; Table 2). Sustained periods of below-average precipitation in large areas of Bolivia and central-northwestern Argentina were also reported by these authors, such as the first four decades of the 18th century, and the transition between the 18th and 19th century (1780–1810). These long drought periods are also present in our 300-year record

Field correlations
δ¹⁸O-Precipitation reconstruction and SADA
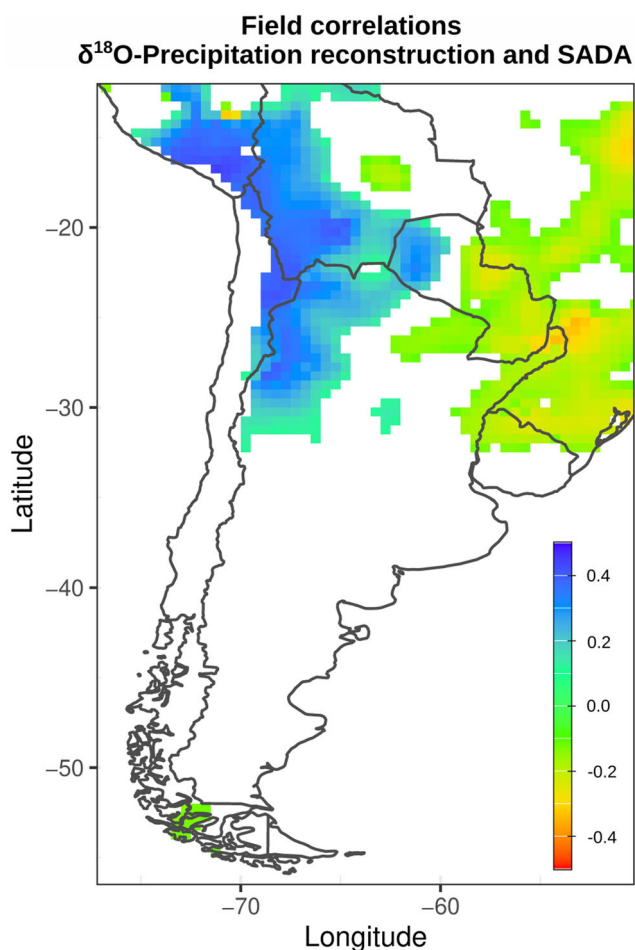
Fig. 6 | Relationship between the precipitation reconstruction and the South American Drought Atlas. Field correlations between our tree-ring $\delta^{18}O$ precipitation reconstruction and the Palmer Drought Severity Index (PDSI) from the South American Drought Atlas for the 1700–1999 period. Only significant values are shown ($p < 0.05$). Correlations were calculated at https://sada.cr2.cl/[100]. The South American Drought Atlas is a gridded drought reconstruction based on tree-ring width chronologies from South America[56].

(1709–1727, 1766–1818; Table 2). The severe drought of 1860–1861 in our reconstruction has been related to notable mortality crises during the years 1861–1863 in the high Andean communities of Rinconada, Santa Catalina and Cochinoca in northwestern Argentina, and Estarca, Talina and Esmoraca in southern Bolivia[60]. The negative effects of this extreme drought may have been exacerbated by the relative prosperity of the region during the previous decades when average to above-average rainfall prevailed (Fig. 3), likely resulting in insufficient planning and preparation for an extended period of drought[60]. Furthermore, historical archives[58] and the new precipitation reconstruction presented in this study, agree on the timing of extreme wet events, and report abundant precipitation from 1700 to 1708, and during 1797.

Atmospheric circulation features retained by the precipitation reconstruction

During the SASM mature phase, convection and diabatic heating over western Amazon, the core region of the SASM, facilitate the formation of an upper-level anticyclonic circulation over Bolivia, called the Bolivian High[61]. This pressure cell weakens the otherwise dominant dry westerlies from the Pacific, resulting in anomalous easterly upper-level circulation over this region, which in turn favours the moisture transport sourced from the Amazon Basin, through turbulent mixing and entrainment of easterly

momentum[27,29]. These circulation features together with increased insolation over the Altiplano, contribute to the development of convective rainfall over this high elevation plateau of the Altiplano, typically between December and March during the peak SASM season[27,62–64]. In the Altiplano, annual minima in $\delta^{18}Op$ correspond to the annual precipitation maxima and coincide with elevated convective activity (lower OLR) and increased easterly flow at 200 hPa[37]. We show a clear link between our $\delta^{18}O$ precipitation reconstruction and 200 hPa zonal wind and OLR variations aloft (Fig. 5d–f), demonstrating that our reconstruction captures the easterly flow and convective activity related with precipitation events over the Altiplano region.

There are some differences in the circulation field between instrumental (Fig. 5b) and reconstructed precipitation (Fig. 5e), reminiscent of the slightly different moisture transport that dominates the northern and southern part of the Altiplano region, as identified in Vuille and Keimig[27]. This suggests that the instrumental precipitation record may be slightly biased toward the central-northern Altiplano, where more meteorological station data is available, while our $\delta^{18}O$-based DJFM reconstruction represents precipitation centred over a slightly more southern location. Nonetheless, the dominance of the easterly moisture transport is apparent in both regression fields. Overall, the spatial relationships between the instrumental precipitation record and OLR and 200hPa wind field are well reproduced by our reconstruction (Fig. 5).

At interannual timescales, the SASM and the moisture transport to the Altiplano are influenced by tropical Pacific SST, with below normal precipitation during El Niño and above normal precipitation during La Niña years[65,66]. Our tree-ring $\delta^{18}O$ chronology captures this ENSO signal, with tree-ring $\delta^{18}O$ correlating positively with tropical Pacific DJFM SST (Fig. 1c). This positive correlation with SST reflects the more enriched tree-ring $\delta^{18}O$ resulting from below normal precipitation in our study region, as well as depleted tree-ring $\delta^{18}O$ being associated with above normal precipitation[33]. Precipitation over the Altiplano also seems to have a decadal signal, coincident with a decadal periodicity in the tropical Pacific SSTs, that is retained by the tree-ring $\delta^{18}O$ chronology, as discussed below.

The decadal signal
A decadal periodicity in our tree-ring $\delta^{18}O$ record is the most prominent cycle and is highly consistent with similar peaks in the instrumental records of precipitation, as well as tropical Pacific SST from the Niño 3.4 and Niño 4 regions (Fig. 2). This decadal cycle is also present in the Altiplano tree-ring width precipitation reconstruction[43], the tropical Andean ice core $\delta^{18}O$[67] and the central-western Pacific coral $\delta^{18}O$ records[15]. Significant periodicities of around 11–14 years are also present in 400-year lake area reconstructions in the southern Altiplano based on lake sediments[68], and on tree-ring width chronologies covering the last six centuries[69]. Coupled decadal cycles lasting 8 to 13 years between ring-width precipitation reconstruction and SST in the Niño 3.4 region have been reported for the last 140 years[43]. Consistent with these findings, the low-frequency $\delta^{18}O$ precipitation reconstruction shows high correlations with decadal oscillations in Altiplano precipitation, and SSTa in the Niño 3.4 and Niño 4 regions, the Andean ice core $\delta^{18}O$ and the Central Pacific coral $\delta^{18}O$ (Fig. 4).

Warmer tropical Pacific SST at decadal time scales have been linked to intensified westerlies at 200 hPa above the Central Andes and enhanced subsidence over the Amazon basin, as a result of a perturbed Walker circulation[70–72]. This subsidence results in reduced convective activity upstream and hence in water vapour being transported to the Andes that is more enriched in ¹⁸O, leading to less negative $\delta^{18}O$ in ice cores and tree rings[36,73] (Fig. 4). Warmer temperatures in the central and western tropical Pacific Ocean are also related to convective activity and increased rainfall in this region, causing depleted coral $\delta^{18}O$ values in the Palmyra Island record[15].

While the linkages between Altiplano precipitation and Pacific SST at decadal timescales dominate over the Altiplano region, the Atlantic Ocean may have some role to play as well. However, the joint influences from the Pacific and Atlantic on these timescales can be difficult to effectively

separate, as the two ocean basins strongly interact with one another[71,72,74]. For example, decadal frequency in the Atlantic Meridional Mode (AMM) with cold (1971–1995) and warm (1925–1970 and 1995–2006) phases of the AMM[75] can be compared with wet and dry phases in our reconstruction respectively (Fig. 3a, Table 2). This can be attributed to a northward displacement of the ITCZ, weakening the moisture influx into the South American Summer Monsoon region, thereby decreasing the available moisture that reaches the Altiplano[75,76]. Taken together, these observations may suggest that the decadal signal of the δ^{18}O paleorecords reflects the joint impacts of teleconnections between central/western tropical Pacific and Atlantic Oceans on the hydroclimate conditions of the tropical Andes at decadal-interdecadal timescales[74,77].

Conclusion

The complexity of tropical South American hydroclimate, the lack of sufficiently long-term instrumental records and the distinct properties of high-resolution paleo-proxies, require integrating multi-proxy records for characterising the full range of past climate variability at different temporal and spatial scales. *Polylepis tarapacana*, the oldest tree species of tropical South America suitable for dendrochronology, provides a highly sensitive precipitation record based on tree-ring δ^{18}O. Our tree-ring δ^{18}O record reflects the local and large-scale circulation patterns related to precipitation in the Altiplano region, allowing us to develop a summer precipitation reconstruction that explains 56% of the inter-annual variability in the instrumental precipitation. Hence the precipitation reconstruction presented here can be used to extend the spatially and temporally limited instrumental record in the region. This multi-centennial tree-ring δ^{18}O record not only captures a large amount of precipitation variability in the Altiplano, but also the atmospheric circulation features and climate forcing related with hydroclimate in this region. A strong decadal signal present in our tree-ring δ^{18}O record is shared with ice core δ^{18}O from the southern tropical Andes and coral δ^{18}O from the tropical Pacific. This coherence shared by in-land Andean and tropical Pacific SST proxies underscores decadal teleconnections and highlights the value of δ^{18}O archives to improve the decadal-scale component of tropical hydroclimate in South America and tropical Pacific SST reconstructions. More measurements of δ^{18}O in tree rings from existing centennial to millennial chronologies in (sub) tropical South America will extend the current spatiotemporal coverage of hydroclimate records leading to improvements in current publicly available databases (e.g., Iso2k Database[78]) with new precisely dated records at an annual resolution.

Methods

Study site and isotope record

The study site is located in the Altiplano, a high-elevation plateau in the tropical Andes between 13° and 23°S with a mean elevation of 3600–4000 m a. s. l. We developed a 314-year tree-ring δ^{18}O chronology using cross-sections from five multi-stem *Polylepis tarapacana* trees collected at the site Uturunco, Bolivia (22.3°S, 67.23°W) at an average elevation of 4650 m a. s. l., on moderate slopes and with sparse canopy density (Fig. 1). These five cross-sections yielded five ring-width series cross-dated against more than 80 ring-width series from the Uturunco site, and their annual resolution validated against an extended *Polylepis tarapacana* ring-width network from the Altiplano[43]. We assigned the calendar date of an annual ring to the year corresponding to the beginning of stem growth, as is common practice in the southern hemisphere[79]. We cut the individual tree rings of each cross-section, extracted cellulose and measured δ^{18}O in cellulose following Andreu-Hayles et al.[80]. No pooling was performed and a total of 1560 rings corresponding to five δ^{18}O values for each year from 1700 to 2013 were measured (Fig. 1a), with the exception of 10 rings (0.6% of the total available rings) that could not be measured due to the low amount of the cellulose material. We assessed the strength of the common signal shared by individual series and the quality of the record through time, by calculating the mean correlation between series (*rbar*), and the Expressed Population Signal

(EPS) for different time windows[81,82]. More comprehensive details regarding the methodology used to develop the tree-ring isotope chronology can be found in Rodriguez-Caton et al.[32,33].

Gridded climate datasets

To characterise the hydroclimate of our study region we retrieved monthly precipitation data from the Climate Hazards Group InfraRed Precipitation with Station (CHIRPS) dataset, available from 1981-present[83] for the summer rainy season comprising December, January, February and March (DJFM) (Fig. 1c). CHIRPS is a blend between remote sensing estimates and in-situ data from meteorological stations, with a spatial resolution of 0.05° × 0.05°. Due to the large precipitation variability in this region, the highly spatially resolved CHIRPS dataset also provided the opportunity to re-scale our station-based precipitation anomalies to millimetres (see section below).

To explore the spatial connections between climate and our tree-ring δ^{18}O record over a longer (1901–2013) period (Fig. 1c), we used summer (DJFM) Climatic Research Unit (CRU) precipitation 0.5° grid resolution version TS 4.05[84] and DJFM global Extended Reconstructed Sea Surface Temperature (ERSST) 2° grid resolution version 5[85] data. We detrended both the monthly CRU and SST data using a linear model before conducting any correlation analysis. SST data were also used for spectral analysis (see section Spectral properties of instrumental and paleo-records). CHIRPS, National Oceanic and Atmospheric Administration interpolated Outgoing Longwave Radiation (OLR)[86], ERA5 reanalysis[87], and the South American Drought Atlas (SADA)[56] were used to assess the main relationships between precipitation and atmospheric circulation patterns with instrumental and reconstructed hydroclimate.

Regional precipitation record from meteorological stations

Total precipitation amount across the Altiplano region shows great spatial heterogeneity due to the complex topography in the Andes[88,89], but shares similar patterns of interannual variability[27,43]. We first selected 114 available precipitation series from weather stations distributed across the Altiplano at elevations higher than 3200 m.a.s.l., located within 650 km from the study site. This search radius is broadly consistent with the spatial scales at which precipitation and cloud cover are correlated. The globally averaged correlation decay distance is 450 km for precipitation, 600 km for cloud cover, and 1200 km for temperature[84]. This slightly larger search radius was necessary due to the low density of the observational network in the region. To then capture regional scale precipitation variability, we further selected stations significantly correlated ($p < 0.05$) with at least twenty of the remaining 113 stations for the summer rainy season (DJFM) and with a minimum time span of 20 years. This resulted in the selection of 38 stations which only shared one year in common, preventing the calculation of anomalies based on a shared common period among stations (see calculation of precipitation anomalies below). To capture a strong and high-quality regional precipitation signal and ensure a representative regional series, a final selection of weather stations was made to include at least three contributing meteorological stations in each year and optimise: i) the total number of stations, ii) the common period among stations, iii) the quality of the stations (less than 25% missing data), and iv) the calibration length for the reconstruction. The final selection included eight weather stations with a total DJFM precipitation amount varying from 30 to 402 mm (Table 1, Fig. 1b).

To account for the variability in precipitation amount, we implemented the following five steps. First, precipitation anomalies were calculated for each individual station based on its mean and standard deviation, over the common period among the eight selected stations (1982–1993). Second, we developed a regional time series of DJFM precipitation by averaging the individual stations' standardised anomalies for the period 1961–2007, which included the highest data quality. Third, we obtained a DJFM CHIRPS precipitation time series in millimetres (mm) for our study area by averaging the total precipitation amount across all grid cells with strong correlation (Pearson r correlation coefficient corresponding to

$p < 0.001$) with our δ^{18}O series (domain shown in Fig. 1b). Fourth, we re-scaled the precipitation anomalies derived from the instrumental series to precipitation in mm based on the mean and variance of the CHIRPS time series. Specifically, we transformed precipitation anomalies to mm by multiplying anomalies by the standard deviation of the DJFM CHIRPS precipitation, and adding the mean of the DJFM CHIRPS precipitation. The mean and variance of the CHIRPS time series used for re-scaling were calculated over the common period 1981-2007. Fifth, we log-transformed the precipitation record in mm (all positive values) to obtain a normally distributed record. We used the log-transformed and normally distributed precipitation time series resulting from the eight meteorological stations as a predictor for our reconstruction.

Spectral properties of instrumental and paleo-records

We explored individual and shared spectral properties of tree-ring δ^{18}O (1700–2013), regional instrumental precipitation, SST records, and related paleorecords. We obtained the DJFM SST time series spanning 1854–2019, by averaging mean DJFM SST anomalies for the Niño 4 and Niño 3.4 regions. We used two methods for power-spectrum estimation: the multi-taper method within the SSA-MTM Toolkit[90] (www.atmos.ucla.edu/tcd/ssa/) and the wavelet transform and wavelet coherence transform methods (R package *biwavelet*[91]). Based on the results of the spectral analysis depicting a shared significant decadal signal in these records (see Results and Fig. 2a, b), we further applied a 9–14-year band-pass filter to the selected time series, using the function pass.filt in the package dplR[92]. We then applied the same filter to the tropical Andean δ^{18}O ice core records that have been reported to have significant decadal scale periodicity[67]. We obtained an ice core δ^{18}O index for the Andes by computing the arithmetic mean[93] of the ice core δ^{18}O records from Quelccaya[17] Huascaran[94], and Sajama[95], selecting the common periods between the tree-ring and ice core δ^{18}O 1700–2009, 1894–1992, and 1949–1997, respectively. We also applied the 9–14-year band-pass filter to an El-Niño sensitive coral δ^{18}O composite record from the Palmyra Island covering the period 1886–2016[15,96]. The coral δ^{18}O is monthly-resolved and values for December through March were averaged to obtain an annually resolved record for DJFM.

We calculated the Pearson correlation coefficients between the 9–14-year band-pass filtered precipitation reconstruction based on tree-ring δ^{18}O and the instrumental- and paleo-records. In order to mitigate the effect of the high autocorrelation of the filtered series while testing for the significance of the correlation coefficient, we calculated the effective numbers of degrees of freedom ν_{eff}[97], applying the following formula:

$$\nu_{eff} = N * (1 - \varphi x * \varphi y)/(1 + \varphi x * \varphi y) \qquad (1)$$

where N is the length of the time series, and φx, φy are the lag-1 autocorrelation coefficients of two time series x, y respectively.

Reconstruction development and statistical methods

Based on our 314-year tree-ring δ^{18}O chronology we built a precipitation reconstruction for the Altiplano region using linear regression. The observational data used to train the reconstruction model was the log-transformed regional precipitation record derived from selected weather stations (see Methods section Regional precipitation record from meteorological stations). The full calibration-validation period was 47 years long, covering 1961–2007 (Fig. 3b). Due to constraints of a relatively short time span to calibrate and validate our reconstruction model, we used a sequential leave-10-out block calibration-validation approach. At each iteration we withheld a block of 10 years and calibrated the model using the remaining 37 years of precipitation data. Subsequently, the performance of the resulting model was validated with the withheld 10 years (see ref.[98] for downloadable R code). For example, the first model was developed using a calibration period of 1971–2007 and validated on precipitation between 1961–1970, while the final model was calibrated on precipitation between 1961–1997 and validated on data between 1998 and 2007. Each resulting reconstructed model was evaluated by calculating the explained variance

through the coefficient of determination or *r-squared* (R^2) during the calibration (CRSQ) and verification (VRSQ) period, and we further calculated the median CRSQ and VRSQ for the 38 models. In a similar way, we also used the reduction of error statistic (VRE), and the coefficient of efficiency (VCE) to evaluate all reconstructed models. VRE and VCE values greater than zero indicate that the reconstruction is robust[99].

The leave-10-out calibration-validation method predicted 38 log-transformed precipitation series for the period 1700–2013, which were subsequently back-transformed to mm using an exponential function. The final reconstruction spanning 1700–2013 was calculated as the median of the back-transformed precipitation time series of all 38 models. This final reconstruction was evaluated using the R^2 between the observed precipitation record (re-scaled to mm using CHIRPS, see Methods section Regional precipitation record from meteorological stations) and the reconstructed precipitation for the whole calibration-validation period 1961–2007.

Comparing the reconstruction with atmospheric circulation and independent paleoclimate records

To assess whether our reconstruction represents the regional features of precipitation and atmospheric circulation across South America, we compared the spatial correlation and regression maps resulting from correlating or regressing observed (based on weather stations) and reconstructed (based on δ^{18}O variations) DJFM precipitation with gridded climate data. Field correlations were calculated between the two precipitation records (observed and reconstructed) and gridded CHIRPS precipitation and interpolated OLR (as indicator of tropical deep convection[86]). Field regression maps were calculated between the same indices and 200 hPa wind and geopotential height from ERA5 reanalysis[87] to characterise the tropospheric circulation aloft for the period 1981–2013. Results are displayed using the NASA-GISS software Panoply.

We also compared our DJFM precipitation reconstruction against the gridded Palmer Drought Severity Index (PDSI) from the SADA that covers the South American continent south of 12°S for the last 600 years[56]. The SADA is based on a network of 286 tree-ring width chronologies, including *Polylepis tarapacana* tree-ring records from the Altiplano and also from the Uturunco site. However, note that chronologies included in the SADA are based on ring width and this product does not include the δ^{18}O tree-ring chronology presented herein. Moreover, the tree-ring δ^{18}O chronology is independent from the ring-width chronology at the Uturunco site (i.e. no significant correlations between both series[32]). Field correlations between the δ^{18}O DJFM precipitation reconstruction and the SADA were calculated for the period 1700–1999 using the South American Drought Atlas Explorer at https://sada.cr2.cl/[100].

References

1. Marengo, J. A. et al. Recent developments on the South American monsoon system. *Int. J. Climatol.* **32**, 1–21 (2012).
2. Cai, W. et al. Climate impacts of the El Niño–Southern Oscillation on South America. *Nat. Rev. Earth Environ.* **1**, 215–231 (2020).
3. Garcia, M., Raes, D., Jacobsen, S. E. & Michel, T. Agroclimatic constraints for rainfed agriculture in the Bolivian Altiplano. *J. Arid Environ.* **71**, 109–121 (2007).
4. Canedo-Rosso, C., Hochrainer-Stigler, S., Pflug, G., Condori, B. & Berndtsson, R. Drought impact in the Bolivian Altiplano agriculture associated with the El Niño-Southern Oscillation using satellite imagery data. *Nat. Hazards Earth Syst. Sci.* **21**, 995–1010 (2021).
5. Eccles, R., Zhang, H. & Hamilton, D. A review of the effects of climate change on riverine flooding in subtropical and tropical regions. *J. Water Clim. Change* **10**, 687–707 (2019).
6. Pinos, J. & Quesada-Román, A. Flood risk-related research trends in latin america and the caribbean. *Water Switz* **14**, 1–14 (2022).
7. Minvielle, M. & Garreaud, R. D. Projecting rainfall changes over the South American Altiplano. *J. Clim.* **24**, 4577–4583 (2011).
8. Neukom, R., Rohrer, M., Calanca, P., Salzmann, N. & Huggel, C. Facing unprecedented drying of the Central Andes? Precipitation variability over the period AD 1000 – 2100. *Environ. Res. Lett.* **10**, 084017 (2015).
9. Vera, C. S., Díaz, L. B. & Saurral, R. I. Influence of anthropogenically-forced global warming and natural Climate variability in the rainfall changes observed over the South American Altiplano. *Front. Environ. Sci.* **7**, 1–14 (2019).
10. Segura, H. et al. Recent changes in the precipitation-driving processes over the southern tropical Andes/western Amazon. *Clim. Dyn.* https://doi.org/10.1007/s00382-020-05132-6 (2020).
11. PAGES Hydro2k Consortium. Comparing proxy and model estimates of hydroclimate variability and change over the Common Era. *Clim. Past* **13**, 1851–1900 (2017).
12. Grothe, P. R. et al. Enhanced El Niño–Southern Oscillation Variability in Recent Decades. *Geophys. Res. Lett.* **47**, 1–8 (2020).
13. O'Connor, G. K. et al. Coral Oxygen Isotopic Records Capture the 2015/2016 El Niño Event in the Central Equatorial Pacific. *Geophys. Res. Lett.* **48**, 1–9 (2021).
14. Walter, R. M. et al. The CoralHydro2k database: a global, actively curated compilation of coral δ18O and Sr/Ca proxy records of tropical ocean hydrology and temperature for the Common Era. *Earth Syst. Sci. Data* **15**, 2081–2116 (2023).
15. Cobb, K. M., Charles, C. D. & Hunter, D. E. A central tropical Pacific coral demonstrates Pacific, Indian, and Atlantic decadal climate connections. *Geophys. Res. Lett.* **28**, 2209–2212 (2001).
16. Vuille, M. et al. A review of the Past South American monsoon history as recorded in stable isotopic proxies over the past two millennia. *Clim. Past* 1309–1321, https://doi.org/10.5194/cp-8-1309-2012 (2012).
17. Thompson, L. G. et al. Annually resolved ice core records of tropical climate variability over the past ~1800 years. *Science* **340**, 945–950 (2013).
18. Orrison, R. et al. South American Summer Monsoon variability over the last millennium in paleoclimate records and isotope-enabled climate models. *Clim. Past* **18**, 2045–2062 (2022).
19. Ballantyne, A. P., Baker, P. A., Chambers, J. Q., Villalba, R. & Argollo, J. Regional Differences in South American Monsoon Precipitation Inferred from the Growth and Isotopic Composition of Tropical Trees. *Earth Interact.* **15**, 1–35 (2011).
20. Brienen, R. J. W., Helle, G., Pons, T. L., Guyot, J.-L. & Gloor, M. Oxygen isotopes in tree rings are a good proxy for Amazon precipitation and El Nino-Southern Oscillation variability. *Proc. Natl. Acad. Sci.* **109**, 16957–16962 (2012).
21. Volland, F., Pucha, D. & Brauning, A. Hydro-climatic variability in southern Ecuador reflected by tree-ring oxygen isotopes. *Erdkunde* **70**, 69–82 (2016).
22. Cintra, B. B. L. et al. Tree - ring oxygen isotopes record a decrease in Amazon dry season rainfall over the past 40 years. *Clim. Dyn.* https://doi.org/10.1007/s00382-021-06046-7 (2021).
23. Pagotto, M. A., Menezes, I. R. N., Costa, C. M., Lisi, C. S. & Bräuning, A. Oxygen isotopes in tree rings of Cedrela odorata L. as an indicator of hydroclimate variations in a seasonally dry tropical forest in northeastern Brazil. *Trees Struct. Funct.* **35**, 1889–1903 (2021).
24. Baker, J. C. A. et al. The Changing Amazon Hydrological Cycle — Inferences From Over 200 Years of Tree-Ring Oxygen Isotope Data Journal of Geophysical Research: Biogeosciences. *J. Geophys. Res. Biogeosci.* https://doi.org/10.1029/2022JG006955 (2022).
25. Vargas, D. et al. ITCZ precipitation and cloud cover excursions control Cedrela nebulosa tree-ring oxygen and carbon isotopes in the northwestern Amazon. *Glob. Planet. Change* **211**, 103791 (2022).
26. Ortega Rodriguez, D. R. et al. Climate variability of the southern Amazon inferred by a multi-proxy tree-ring approach using Cedrela fissilis Vell. *Sci. Total Environ.* **871**, 162064 (2023).
27. Vuille, M. & Keimig, F. Interannual variability of summertime convective cloudiness and precipitation in the central Andes derived from ISCCP-B3 data. *J. Clim.* **17**, 3334–3348 (2004).
28. Garreaud, R. D. Multiscale analysis of the summertime precipitation over the central Andes. *Mon. Weather Rev.* **127**, 901–921 (1999).
29. Garreaud, R., Vuille, M. & Clement, A. C. The climate of the Altiplano: Observed current conditions and mechanisms of past changes. *Palaeogeogr. Palaeoclimatol. Palaeoecol.* **194**, 5–22 (2003).
30. Segura, H. et al. New insights into the rainfall variability in the tropical Andes on seasonal and interannual time scales. *Clim. Dyn.* **53**, 405–426 (2019).
31. Vuille, M. & Werner, M. Stable isotopes in precipitation recording South American summer monsoon and ENSO variability: Observations and model results. *Clim. Dyn.* **25**, 401–413 (2005).
32. Rodriguez-Caton, M. et al. Different climate sensitivity for radial growth, but uniform for tree-ring stable isotopes along an aridity gradient in Polylepis tarapacana, the world's highest elevation tree species. *Tree Physiol* **41**, 1353–1371 (2021).
33. Rodriguez-Caton, M. et al. Hydroclimate and ENSO Variability Recorded by Oxygen Isotopes from Tree Rings in the South American Altiplano. *Geophys. Res. Lett.* **49**, 1–11 (2022).
34. Risi, C., Bony, S. & Vimeux, F. Influence of convective processes on the isotopic composition (δ18O and δD) of precipitation and water vapor in the tropics: 2. Physical interpretation of the amount effect. *J. Geophys. Res. Atmospheres* **113**, 1–12 (2008).
35. Samuels-Crow, K. et al. Upwind convective influences on the isotopic composition of atmospheric water vapor over the tropical Andes. *J. Geophys. Res. Atmospheres* **119**, 7051–7063 (2014).
36. Hurley, J. V., Vuille, M. & Hardy, D. R. On the Interpretation of the ENSO Signal Embedded in the Stable Isotopic Composition of Quelccaya Ice Cap, Peru. *J. Geophys. Res. Atmospheres* **124**, 131–145 (2019).
37. Fiorella, R. P. et al. Spatiotemporal variability of modern precipitation δ18O in the central Andes and implications for paleoclimate and paleoaltimetry estimates. *J. Geophys. Res. Atmospheres* **120**, 1–27 (2015).
38. Allen, S. T., Sprenger, M., Bowen, G. J. & Brooks, J. R. Spatial and Temporal Variations in Plant Source Water: O and H Isotope Ratios from Precipitation to Xylem Water. in *Stable Isotopes in Tree Rings: Inferring Physiological, Climatic and Environmental Responses* (eds. Siegwolf, R. T. W., Brooks, J. R., Roden, J. & Saurer, M.) 501–535 (Springer International Publishing, Cham, 2022). https://doi.org/10.1007/978-3-030-92698-4_18.
39. Craig, H. & Gordon, L. Deuterium and oxygen-18 variations in the ocean and the marine atmosphere. in *Proceedings of a Conference on Stable Isotopes in Oceanographic Studies and Paleotemperatures* (ed. Tongiorgi, E.) 9–130 (Spoleto, Italy, 1965).
40. Roden, J. S., Lin, G. & Ehleringer, J. R. A mechanistic model for interpretation of hydrogen and oxygen isotope ratios in tree-ring cellulose. *Geochim. Cosmochim. Acta* **64**, 21–35 (2000).

41. Cheesman, A. W. & Cernusak, L. A. Infidelity in the outback: Climate signal recorded in Δ18O of leaf but not branch cellulose of eucalypts across an Australian aridity gradient. *Tree Physiol.* **37**, 554–564 (2017).

42. Argollo, J., Soliz, C. & Villalba, R. Potencialidad dendrocronológica de Polylepis tarapacana en los Andes Centrales de Bolivia Dendrocronological potential of Polylepis tarapacana in the Central Andes of Bolivia. *Ecol. En Boliv.* **39**, 5–24 (2004).

43. Morales, M. S. et al. Precipitation changes in the South American Altiplano since 1300 AD reconstructed by tree-rings. *Clim. Past* **8**, 653–666 (2012).

44. Morales, M. S. et al. Drought increase since the mid-20th century in the northern South American Altiplano revealed by a 389-year precipitation record. *Clim. Past* **19**, 457–476 (2023).

45. Solíz, C. et al. Spatio-temporal variations in Polylepis tarapacana radial growth across the Bolivian Altiplano during the 20th century. *Palaeogeogr. Palaeoclimatol. Palaeoecol.* **281**, 296–308 (2009).

46. Vystavna, Y., Matiatos, I. & Wassenaar, L. I. Temperature and precipitation effects on the isotopic composition of global precipitation reveal long-term climate dynamics. *Sci. Rep.* **11**, 1–9 (2021).

47. Baker, J. C. A. et al. Oxygen isotopes in tree rings show good coherence between species and sites in Bolivia. *Glob. Planet. Change* **133**, 298–308 (2015).

48. Lavergne, A. et al. Are the oxygen isotopic compositions of Fitzroya cupressoides and Nothofagus pumilio cellulose promising proxies for climate reconstructions in northern Patagonia? *J. Geophys. Res. Biogeosci.* 1–10, https://doi.org/10.1002/2015JG003260 (2016).

49. Grießinger, J. et al. Imprints of climate signals in a 204 year δ18O tree-ring record of nothofagus pumilio from Perito Moreno Glacier, Southern Patagonia (50◦S). *Front. Earth Sci.* **6**, 1–17 (2018).

50. Locosselli, G. M. et al. Intra-annual oxygen isotopes in the tree rings record precipitation extremes and water reservoir levels in the Metropolitan Area of São Paulo, Brazil. *Sci. Total Environ.* **743**, 140798 (2020).

51. Meier, W. J. H. et al. A tree-ring δ18O series from southernmost Fuego-Patagonia is recording flavors of the Antarctic Oscillation. *Glob. Planet. Change* **195**, 103302 (2020).

52. Penchenat, T. et al. Tree-ring isotopes from Araucaria araucana as useful proxies for climate reconstructions. *Dendrochronologia* **74**, 125979 (2022).

53. Soto-Rogel, P., Aravena, J. C., Villalba, R., Meier, W. J. H. & Grießinger, J. Tree-ring δ18Ocellulose variations in two Nothofagus species record large-scaleclimatic signals in the South American sector of the Southern Ocean. *Palaeogeogr. Palaeoclimatol. Palaeoecol.* **617**, 111474 (2023).

54. Bird, B. W. et al. A 2,300-year-long annually resolved record of the South American summer monsoon from the Peruvian Andes. *Proc. Natl. Acad. Sci.* **108**, 8583–8588 (2011).

55. Apaéstegui, J. et al. Precipitation changes over the eastern Bolivian Andes inferred from speleothem (δ18O) records for the last 1400 years. *Earth Planet. Sci. Lett.* **494**, 124–134 (2018).

56. Morales, M. S. et al. 600 years of South American tree rings reveal an increase in severe hydroclimatic events since mid-20th century. *PNAS* 1–48, https://doi.org/10.1073/pnas.2002411117 (2020).

57. Gioda, A., Prieto, M. & del, R. Histoire des sécheresses Andines Potosi, El Niño et le petit âge glaciaire. *La Météorologie* **8**, 33–42 (1999).

58. Prieto, M. R., Herrera, R. & Dussel, P. Archival Evidence for some Aspects of Historical Climate Variability in Argentina and Bolivia During the 17 and 18 Centuries. In *Southern Hemisphere Paleo- and Neoclimates* 127–142 (Springer, Berlin, Heidelberg, 2000). https://doi.org/10.1007/978-3-642-59694-0_8.

59. Prieto, M., del, R. & García Herrera, R. Documentary sources from South America: Potential for climate reconstruction. *Palaeogeogr. Palaeoclimatol. Palaeoecol.* **281**, 196–209 (2009).

60. Gil Montero, R. & Villalba, R. Tree rings as a surrogate for economic stress - An example from the Puna of Jujuy, Argentina in the 19th century. *Dendrochronologia* **22**, 141–147 (2005).

61. Lenters, J. D. & Cook, K. H. On the origin of the Bolivian high and related circulation features of the South American climate. *J. Atmospheric Sci.* **54**, 656–677 (1997).

62. Garreaud, R. D. & Aceituno, P. Interannual rainfall variability over the South American Altiplano. *J. Clim.* **14**, 2779–2789 (2001).

63. Falvey, M. & Garreaud, R. D. Moisture variability over the South American Altiplano during the South American low level jet experiment (SALLJEX) observing season. *J. Geophys. Res. Atmospheres* **110**, 1–12 (2005).

64. Espinoza, J. C. et al. Hydroclimate of the Andes Part I: Main Climatic Features. *Front. Earth Sci.* **8**, 1–20 (2020).

65. Vuille, M. Atmospheric circulation over the Bolivian Altiplano during dry and wet periods and extreme phases of the southern oscillation. *Int. J. Climatol.* **19**, 1579–1600 (1999).

66. Sulca, J., Takahashi, K., Espinoza, J. C., Vuille, M. & Lavado-Casimiro, W. Impacts of different ENSO flavors and tropical Pacific convection variability (ITCZ, SPCZ) on austral summer rainfall in South America, with a focus on Peru. *Int. J. Climatol.* **38**, 420–435 (2018).

67. Melice, J. L. & Roucou, P. Decadal time scale variability recorded in the Quelccaya summit ice core δ18O isotopic ratio series and its relation with the sea surface temperature. *Clim. Dyn.* **14**, 117–132 (1998).

68. Santamans, C. D., Cordoba, F. E., Franco, M. G., Vignoni, P. & Lupo, L. C. Hydro-climatological variability in Lagunas de Vilama System, Argentinean Altiplano-Puna Plateau, Southern Tropical Andes (22° S), and its response to large-scale climate forcings. *Sci. Total Environ.* **767**, 144926 (2021).

69. Morales, M. S., Carilla, J., Grau, H. R. & Villalba, R. Multi-century lake area changes in the Southern Altiplano: a tree-ring-based reconstruction. *Clim. Past* **11**, 1139–1152 (2015).

70. Segura, H., Espinoza, J. C., Junquas, C. & Takahashi, K. Evidencing decadal and interdecadal hydroclimatic variability over the Central Andes. *Environ. Res. Lett.* **11**, 094016 (2016).

71. Sulca, J., Vuille, M. & Dong, B. Interdecadal variability of the austral summer precipitation over the Central Andes. *Front. Earth Sci.* 1–22, https://doi.org/10.3389/feart.2022.954954 (2022).

72. Sulca, J., Takahashi, K., Tacza, J., Espinoza, J. & Dong, B. Decadal variability in the austral summer precipitation over the Central Andes: Observations and the empirical-statistical downscaling model. *Int. J. Climatol.* 1–29, https://doi.org/10.1002/joc.7867 (2022).

73. Bradley, R. S., Vuille, M., Hardy, D. & Thompson, L. G. Low latitude ice cores record Pacific sea surface temperatures. *Geophys. Res. Lett.* **30**, 2–5 (2003).

74. He, Z., Dai, A. & Vuille, M. The joint impacts of Atlantic and Pacific multidecadal variability on South American precipitation and temperature. *J. Clim.* **34**, 7959–7981 (2021).

75. Canedo-Rosso, C., Uvo, C. B. & Berndtsson, R. Precipitation variability and its relation to climate anomalies in the Bolivian Altiplano. *Int. J. Climatol.* **39**, 2096–2107 (2019).

76. Flantua, S. G. A. et al. Climate variability and human impact in South America during the last 2000 years: Synthesis and perspectives from pollen records. *Clim. Past* **12**, 483–523 (2016).

77. Jenkins, H. S. Amazon climate reconstruction using growth rates and stable isotopes of tree ring cellulose from the madre de dios basin, Peru (2009). Dissertation, Duke University. Retrieved from https://hdl.handle.net/10161/1352.

78. Konecky, B. L. et al. The Iso2k database: A global compilation of paleo-δ18O and δ2H records to aid understanding of Common Era climate. *Earth Syst. Sci. Data* **12**, 2261–2288 (2020).

79. Schulman, E. Longevity under adversity in conifers. *Science* **119**, 883–884 (1954).

80. Andreu-Hayles, L. et al. A high yield cellulose extraction system for small whole wood samples and dual measurement of carbon and oxygen stable isotopes. *Chem. Geol.* **504**, 53–65 (2019).

81. Wigley, T. M. L., Briffa, K. R. & Jones, P. D. On the average value of correlated time series, with applications in dendroclimatology and hydrometeorology. *J. Clim. Appl. Meteorol.* **23**, 201–213 (1984).

82. Briffa, K. R. Interpreting high-resolution proxy climate data- the example of dendroclimatology. In *Analysis of climate variability, applications of statistical techniques* (eds. Von Storch, H. & Navarra, A.) 77–94 (Springer, Berlin, 1995).

83. Funk, C. et al. The climate hazards infrared precipitation with stations - A new environmental record for monitoring extremes. *Sci. Data* **2**, 1–21 (2015).

84. Harris, I., Osborn, T. J., Jones, P. & Lister, D. Version 4 of the CRU TS monthly high-resolution gridded multivariate climate dataset. *Sci. Data* **7**, 1–18 (2020).

85. Huang, B. et al. NOAA Extended Reconstructed Sea Surface Temperature (ERSST), Version 5. https://doi.org/10.7289/V5T72FNM (2017).

86. Liebmann, B. & Smith, C. A. Description of a Complete (Interpolated) Outgoing Longwave Radiation Dataset. *Bull. Am. Meteorol. Soc.* **77**, 1275–1277 (1996).

87. Hersbach, H. et al. ERA5 monthly averaged data on pressure levels from 1940 to present. Copernicus Climate Change Service (C3S) Climate Data Store (CDS) https://doi.org/10.24381/cds.6860a573 (2023).

88. Huerta, A. & Lavado-Casimiro, W. Trends and variability of precipitation extremes in the Peruvian Altiplano (1971–2013). *Int. J. Climatol.* **41**, 513–528 (2021).

89. Torres-Batlló, J. & Martí-Cardona, B. Precipitation trends over the southern Andean Altiplano from 1981 to 2018. *J. Hydrol.* **590**, 125485 (2020).

90. Ghil, M. et al. Advanced Spectral Methods for Climatic Time Series. *Rev. Geophys* **40**, 3.1–3.41 (2002).

91. Gouhier, T., Grinsted, A. & Simko, V. R package biwavelet: Conduct Univariate and Bivariate Wavelet Analyses (Version 0.20.21) (2021). https://github.com/tgouhier/biwavelet.

92. Bunn, A. G. A dendrochronology program library in R (dplR). *Dendrochronologia* **26**, 115–124 (2008).

93. Hoffmann, G. et al. Coherent isotope history of Andean ice cores over the last century. *Geophys. Res. Lett.* **30**, 1–4 (2003).

94. Thompson, L. G. et al. Late glacial stage and holocene tropical ice core records from Huascarán, Peru. *Science* **269**, 46–50 (1995).

95. Thompson, L. G. et al. A 25,000-year tropical climate history from Bolivian ice cores. *Science* **282**, 1858–1864 (1998).

96. Sanchez, S. C. et al. A Continuous Record of Central Tropical Pacific Climate Since the Midnineteenth Century Reconstructed From Fanning and Palmyra Island Corals: A Case Study in Coral Data Reanalysis. *Paleoceanogr. Paleoclimatology* **35**, 1–15 (2020).

97. Hu, J., Emile-Geay, J. & Partin, J. Correlation-based interpretations of paleoclimate data – where statistics meet past climates. *Earth Planet. Sci. Lett.* **459**, 362–371 (2017).

98. Davi, N. K. et al. Accelerated Recent Warming and Temperature Variability Over the Past Eight Centuries in the Central Asian Altai From Blue Intensity in Tree Rings. *Geophys. Res. Lett*. **48**, e2021GL092933 (2021).

99. Cook, E. R. et al. Asian Monsoon Failure and Megadrought During the Last Millennium. *Science.* **328**, 486–489 (2010).

100. Ferrada, A. et al. Explorador del Atlas de Sequías de Sudamérica, Centro de Ciencia del Clima y la Resiliencia (CR)², https://sada.cr2.cl (2021).

101. Hunziker, S. et al. Effects of undetected data quality issues on climatological analyses. *Clim. Past* **14**, 1–20 (2018).

Acknowledgements

Author contributions

M.R.-C., L.A.-H., M.S.M., V.D., and R.V. design the study. M.R.-C., T.N. and R.O. processed the tree-ring isotopic data. M.R.-C. performed the experiments and statistical analyses with contributions from M.P.R., M.V, M.S.M., L.A.-H., D.A.C. and A.M.V.-C. M.R.-C. drafted the manuscript with contributions from L.A.-H. L.A.-H., V.D., M.V., M.P.R., D.A.C., M.S.M. and J.A.R., contributed to data interpretation. M.R.-C., M.S.M., M.P.R., T.N., M.V., J.A.R., R.O., D.A.C., A.M.V.-C., M.E.F., T.M., V.D., R.V. and L.A.-H. contributed to reading, writing, and editing the manuscript.

Competing interests

The authors declare no competing interests.

Additional information